

Shear Behavior of Non-dilative Interfaces: New Insights from Multiscale Experiments

LALIT KANDPAL



**Department of Civil Engineering
INDIAN INSTITUTE OF TECHNOLOGY DELHI**

JANUARY 2025

© **Indian Institute of Technology Delhi (IITD), New Delhi, 2025**

**Shear Behavior of Non-dilative Interfaces: New
Insights from Multiscale Experiments**

by

LALIT KANDPAL

Department of Civil Engineering

Submitted

in fulfillment of requirements of the degree of

DOCTOR OF PHILOSOPHY

to the



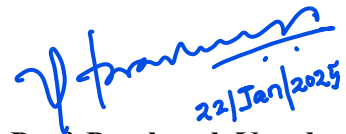
INDIAN INSTITUTE OF TECHNOLOGY DELHI

JANUARY 2025

Dedicated to my Family

CERTIFICATE

This is to certify that the thesis entitled "SHEAR BEHAVIOR OF NON-DILATIVE INTERFACES: NEW INSIGHTS FROM MULTISCALE EXPERIMENTS" is being submitted by Mr. Lalit Kandpal in the fulfillment for the award of the degree of Doctor of Philosophy to the Indian Institute of Technology Delhi. This thesis is the record of the research work and is entirely carried out by him under my supervision and guidance. The research report and results presented in this thesis have not been submitted, in part or full, to any University or Institute for the award of any degree or diploma.



Prof. Prashanth Vangla
Associate Professor
Department of Civil Engineering
Indian Institute of Technology Delhi
New Delhi - 110016
INDIA

ACKNOWLEDGEMENT

Any achievement is the result of the efforts of many individuals, and this PhD work is no exception. I am deeply grateful to all those who have supported and inspired me throughout my PhD journey.

First and foremost, I extend my heartfelt thanks to my supervisor, **Prof. Prashanth Vangla**, for his invaluable guidance, unwavering support, and insightful feedback throughout the research process. His expertise, enthusiasm, and encouragement have been pivotal in shaping the direction and scope of this thesis.

To the members of my research committee, **Prof. B. J. Alappat**, **Prof. G. V. Ramana**, and **Prof. Vivek Buwa**, for their constructive feedback and valuable insights, which have significantly enriched this work.

To the staff and faculty of the **Department of Civil Engineering** at IIT Delhi, particularly **Mr. Manoj Kumar Neelam**, **Mr. Alok Kumar**, **Mr. Lokendra Singh Dangi**, **Mr. Ram Janam**, and **Mr. Manish** from the Geotechnical and Rock Engineering division, for their assistance, support, and provision of essential resources and administrative help.

I am grateful to the **Science and Engineering Research Board (SERB)** for their financial support, which allowed me to conduct my research efficiently and hassle-free.

I also extend my thanks to the **Port and Airport Research Institute**, with special appreciation to **Dr. Satoshi Matsumura**, for providing me with the opportunity to use their facilities. Additionally, I thank **Prof. Nitya Nand Gosvami** of the Department of Materials Science at IIT Delhi for granting access to their facilities for conducting our experiments. I extend my sincere gratitude to **Aimil Ltd.** for their support during the

manufacturing of my apparatus. Special thanks to **Ms. Aarti Bhargava** for her consistent support and availability throughout the process, and to **Mr. Anil Kumar Chaudhary and Mr. Abhishek Anand** for their assistance during the testing phase of the apparatus.

To my friends and colleagues—**Gayathri Venu Latha, Rituraj Devrani, Dipali Jindal, Satyam Dey, Aayush Kumar, Harsha Vardhan Kurugodu, Akshansh Khare, Apoorva Agarwal, Garima Gupta, Sujata Fulambarkar, Mayuresh Bakare, Ashwinth Raj, Mohit Somani, Brijesh Wala, Sateeshkanth S. M., Shashank Shekhar, Kamal Biswas, Abhishek Singh, Prateek Singh, and Aryan Raj** — your steadfast support, encouragement, and camaraderie have made this challenging PhD journey not only bearable but also enjoyable.

I owe a profound debt of gratitude to my incredible family. To my paternal grandparents, **Mr. K.R. Kandpal** and **Mrs. Durga Devi**, whose memory continues to inspire me every day. My heartfelt appreciation goes to my maternal grandparents, **Mr. A. B. Papanai** and **Mrs. Sharda Devi**, my parents, **Mr. M. C. Kandpal** and **Mrs. Deepa Kandpal**, my brother-in-law **Rakesh Joshi**, my cousins **Vaibhav, Vaishali, Ashish, Nidhi**, and my nephew **Vihaan Joshi**. Their unwavering love, support, and encouragement have been a constant source of strength and motivation throughout this journey. Special thanks to my uncles, **M. C. Papanai** and **N. C. Kabdwal**, and my aunts, **Kiran Papanai** and **Geeta Kabdwal**, whose love and support have significantly eased my journey from childhood to the present.

Lastly, I am deeply grateful to my wonderful sister, **Neelam Kandpal**. Her guidance, belief, and constant support have been invaluable, and no words can fully express my gratitude. I feel truly blessed to have a sister like you.

To all of you, I extend my deepest thanks for being part of this journey and making it a memorable and rewarding experience.

ABSTRACT

The interaction at the interface of particulate and continuum materials in composite geotechnical structures can significantly impact their energy efficiency, stability, and performance. Non-dilative interfaces, crucial for many geotechnical structures, require thorough characterization due to their vulnerability as potential failure planes. Understanding the shear behavior of a non-dilative interface system requires studying fundamental aspects that govern the macro aspects through the sliding and plowing of particulate materials on the surface of the continuum material at a micro-level that falls under tribology. While the field of tribology offers extensive insights into friction and wear, its application to geotechnical composite systems remains limited. A comprehensive understanding of particulate kinematics and tribological mechanisms is crucial for assessing shear responses at non-dilative interfaces, particularly within the discipline of geotribology.

This study focuses on investigating the shear behavior of non-dilative interfaces using multiscale experiments. It examines how influential parameters, such as particle morphology, shear-induced surface changes, particle kinematics during shearing, and relative hardness, affect this behavior. To this end, the study proposes novel approaches for accurately characterizing particle shape and shear-induced surface changes. Additionally, two custom-designed apparatuses were developed to gain insights into particle kinematics, micromechanical aspects, and data-driven models for understanding the shear response under different influential parameters and predicting the interface friction angle for geomaterial contacts. The novel 3D shape characterization method developed could quantify the shape (including meso and macro features) and the kinematic behavior of particulate materials using newly introduced

factors. Unlike selective locations, the proposed technique offers the characterization of surface roughness of the entire shear-induced area and provides insights into the shear response. A custom-designed advanced interface shear apparatus was developed to facilitate image analysis of the interaction between particulate and continuum materials from the bottom of the interface plane during shearing for different test setups (fixed or conventional). Through image analysis, the experiments aimed to understand particle kinematics and its influence on sliding and plowing during shearing at the AS interface, which was subsequently leveraged to interpret the shear responses of continuum materials, including high-density polyethylene geomembrane (HDPE), polyvinyl chloride geomembrane (PVC), and stainless steel (ST) with particulate materials of different morphologies under varying normal stresses. Further, direct shear tests with X-ray CT scanning were conducted on similarly sized sands and opaque polymeric materials (HDPE and PVC) under varying normal stresses to validate the insights obtained regarding particle kinematics at the interface using image analysis.

The image and micro-topographical analysis of the tested interfaces reveal that the box fixity, particle shape, and normal stress influence particle kinematics and shear-induced surface changes. The restricted particle movements are observed more for the fixed box than the conventional box. Continuum material properties affect shear response and shear-induced surface roughness values, influenced by hardness and interlayer or junction shear resistance. In interface shear tests on AS and HDPE, considerable plowing is observed for SA_S and R_GB with different critical normal stresses. Despite this, acrylic and geomembrane surfaces show similar frictional behavior and shear-induced surface changes under the same conditions. Particle kinematics for AS provides insights into interactions with geomembranes and materials with similar hardness. HDPE and PVC also exhibit similar kinematic trends in X-ray CT analysis, supporting

these findings. Angular and smooth spherical particles exhibit lesser kinematics despite a huge difference in the shape and shear-induced surface changes. Rough spherical particles have larger displacements and shear-induced surface changes than smooth spherical particles. These findings highlight the crucial role of particle shape and contact stresses in particle kinematics at the interface.

A custom-built micromechanical testing apparatus enables the study of rolling and sliding friction across various geomaterial contacts. The apparatus allows the investigation of rolling and sliding friction of various geomaterial contacts under various testing parameters, including normal load, displacement rate, and dry and wet conditions. The device is instrumented with sensors (load, displacement, and camera) and a computerized data acquisition system to measure and record the force, displacement, and images of the contacts during the test for in-depth study. The images are captured from the bottom of the sliding platform while shearing only for the contacts made of particle and transparent continuum materials. The accuracy of the shear response of geomaterial contacts tested in custom-built micromechanical apparatus is demonstrated by comparing the results of the same contacts obtained from high-end tribometer apparatus. Test findings show that the custom-built apparatus is as accurate as those from a high-end tribometer and reliable for micromechanical geomaterial interaction analysis. Further, experiments are performed on different types of interface contacts and under different conditions to demonstrate the apparatus's sensitivity. The findings indicate that the apparatus stiffness is sufficient, facilitates the understanding of micromechanical behavior, and estimates primary yet essential inputs required to comprehend the complex behavior of geomaterials.

Micromechanical interface shear tests were conducted on scanned particles, highlighting the significant influence of particles' average surface roughness, normal

load, and type of continuum material on the shear response at the particle scale. Spearman's rank correlation coefficient analysis shows a strong correlation between the hardness of the continuum material and the average roughness of particles ($S_{a_particle}$) measured without any filter, highlighting their interdependence in influencing interface shear responses in non-dilative interfaces. The friction coefficient's response to average surface roughness varies across three continuum materials, with PVC exhibiting the highest friction coefficient values, followed by HDPE and ST under similar testing conditions. HDPE's friction coefficient demonstrates exponential growth with $S_{a_particle}$, reflected in increasing b_p values as the normal load increases. Conversely, PVC exhibits a power-law relationship, where the friction coefficient's rate of increase diminishes at higher $S_{a_particle}$ due to minimal surface deformation under increased normal loads. In ST, the friction coefficient shows nearly constant growth with $S_{a_particle}$, indicated by constant m values for the linear fit on the data. Various machine learning models were employed to identify the optimal predictive model using micromechanical experimental data, with the RF model outperforming others by achieving an R^2 of 0.94 for training and 0.89 for testing, thus meeting all validation criteria and being deemed fully acceptable.

सारांश

कणीय और सतत सामग्री के बीच संपर्क का प्रभाव मिश्रित भू-तकनीकी संरचनाओं की ऊर्जा दक्षता, स्थिरता और प्रदर्शन पर महत्वपूर्ण होता है। गैर-प्रसारशील संपर्क, जो कई भू-तकनीकी संरचनाओं के लिए आवश्यक होते हैं, संभावित विफलता के स्थान होने के कारण गहन अध्ययन की आवश्यकता रखते हैं। गैर-प्रसारशील संपर्क प्रणाली के कतरनी व्यवहार को समझने के लिए उन बुनियादी पहलुओं का अध्ययन करना आवश्यक है जो सूक्ष्म स्तर पर सतत सामग्री की सतह पर कणीय पदार्थों के फिसलने और खिसकने के माध्यम से व्यापक पहलुओं को नियंत्रित करते हैं, जो कि घर्षण विज्ञान (ट्राइबोलॉजी) के अंतर्गत आता है। ट्राइबोलॉजी का क्षेत्र घर्षण और घिसाव पर व्यापक अंतर्दृष्टि प्रदान करता है, लेकिन भू-तकनीकी मिश्रित प्रणालियों में इसका उपयोग सीमित है। कणीय गतिकी और ट्राइबोलॉजिकल तंत्रों की गहन समझ गैर-प्रसारशील संपर्कों पर कतरनी प्रतिक्रियाओं का मूल्यांकन करने के लिए महत्वपूर्ण है, विशेष रूप से भू-ट्राइबोलॉजी के क्षेत्र में।

यह अध्ययन गैर-प्रसारशील संपर्कों के कतरनी व्यवहार की जांच पर केंद्रित है, जिसमें प्रभावकारी मापदंडों जैसे कण आकृति, कतरनी-प्रेरित सतह परिवर्तन, कतरनी के दौरान कण गतिकी, और सापेक्ष कठोरता के प्रभाव को शामिल किया गया है। इसके लिए, अध्ययन में कण आकृति और कतरनी-प्रेरित सतह परिवर्तनों को सटीक रूप से वर्णित करने के लिए नए दृष्टिकोणों का प्रस्ताव दिया गया है। इसके अतिरिक्त, कण गतिकी, सूक्ष्म यांत्रिक पहलुओं, और विभिन्न प्रभावकारी मापदंडों के तहत कतरनी प्रतिक्रिया को समझने और भू-सामग्री संपर्कों के लिए इंटरफेस घर्षण कोण की भविष्यवाणी करने के लिए दो कस्टम-डिज़ाइन किए गए उपकरण विकसित किए गए। विकसित 3डी आकृति वर्णनात्मक विधि कणीय सामग्रियों की आकृति (मेसो और मैक्रो विशेषताओं सहित) और कतरनी के दौरान उनकी गतिकी को नए कारकों का उपयोग करके

मापने में सक्षम है। यह प्रस्तावित तकनीक चयनात्मक स्थानों के बजाय पूरे कतरनी-प्रेरित क्षेत्र की सतह खुरदरीपन की विशेषता प्रस्तुत करती है और कतरनी प्रतिक्रिया के बारे में अंतर्दृष्टि प्रदान करती है। कस्टम-डिज़ाइन किए गए उन्नत इंटरफेस कतरनी उपकरण का विकास किया गया, जो कणीय और सतत सामग्रियों के बीच संपर्क का छवि विश्लेषण कतरनी के दौरान इंटरफेस विमान के निचले भाग से अलग-अलग सेटअप (फिक्स्ड या पारंपरिक) के लिए सक्षम बनाता है। छवि विश्लेषण के माध्यम से, इन परीक्षणों का उद्देश्य कण गतिकी और कतरनी के दौरान फिसलने और खिसकने पर इसके प्रभाव को समझना था। यह जानकारी उच्च-घनत्व पॉलीइथाइलीन जियोमेम्ब्रेन (HDPE), पॉलीविनाइल क्लोराइड जियोमेम्ब्रेन (PVC), और स्टेनलेस स्टील (ST) जैसे सतत सामग्रियों के कतरनी प्रतिक्रियाओं की व्याख्या के लिए उपयोग की गई। इसके अलावा, समान आकार के रेत और अपारदर्शी बहुलक सामग्रियों (HDPE और PVC) पर विभिन्न सामान्य तनावों के तहत सीधे कतरनी परीक्षण और X-ray CT स्कैनिंग का उपयोग करके कण गतिकी की जानकारी की पुष्टि की गई।

परीक्षण सतहों के छवि और सूक्ष्म-टोपोग्राफिकल विश्लेषण से पता चला कि बॉक्स का स्थिरता, कण का आकार, और सामान्य तनाव कण गतिकी और कतरनी-प्रेरित सतह परिवर्तनों को प्रभावित करते हैं। फिक्स्ड बॉक्स की तुलना में पारंपरिक बॉक्स में कणों की गति अधिक सीमित पाई गई। सतत सामग्रियों के गुण कतरनी प्रतिक्रिया और कतरनी-प्रेरित सतह खुरदरीपन के मानों को प्रभावित करते हैं, जिसमें कठोरता और इंटरलेयर या जंक्शन कतरनी प्रतिरोध शामिल हैं। AS और HDPE के इंटरफेस कतरनी परीक्षण में, SA_S और R_GB के लिए विभिन्न क्रिटिकल सामान्य तनावों के साथ महत्वपूर्ण खिसकाव देखा गया। इसके बावजूद, ऐक्रेलिक और जियोमेम्ब्रेन सतहें समान घर्षणीय व्यवहार और समान कतरनी-प्रेरित सतह परिवर्तन दिखाती हैं। AS के लिए कण गतिकी जियोमेम्ब्रेन और समान कठोरता वाली सामग्रियों के साथ इंटरफेस पर अंतर्दृष्टि प्रदान करती है। HDPE और PVC में X-ray CT विश्लेषण में समान गतिकी प्रवृत्तियां

प्रदर्शित की गई, जो इन निष्कर्षों का समर्थन करती हैं। विभिन्न आकारों और सतह खुरदरापन वाले कणों का परीक्षण कतरनी व्यवहार को समझने के लिए किया गया। इस अध्ययन ने यह स्थापित किया कि कण आकृति, सामान्य तनाव, और सतत सामग्रियों की कठोरता इंटरफेस पर कण गतिकी को कैसे प्रभावित करती है।

एक कस्टम-निर्मित माइक्रोमैकेनिकल परीक्षण उपकरण विभिन्न भू-सामग्री संपर्कों के बीच रोलिंग और स्लाइडिंग घर्षण का अध्ययन करने में सक्षम बनाता है। यह उपकरण विभिन्न परीक्षण मापदंडों जैसे सामान्य भार, विस्थापन दर, और सूखी और गीली परिस्थितियों के तहत विभिन्न भू-सामग्री संपर्कों के रोलिंग और स्लाइडिंग घर्षण की जांच की अनुमति देता है। इस डिवाइस को सेंसर (भार, विस्थापन, और कैमरा) और एक कंप्यूटरकृत डेटा अधिग्रहण प्रणाली से सुसज्जित किया गया है, जो परीक्षण के दौरान संपर्कों के बल, विस्थापन और छवियों को मापने और रिकॉर्ड करने के लिए सक्षम बनाता है। छवियां केवल उन संपर्कों के लिए शीयरिंग के दौरान स्लाइडिंग प्लेटफॉर्म के नीचे से कैप्चर की जाती हैं, जो कण और पारदर्शी सतत सामग्रियों से बने होते हैं। कस्टम-निर्मित माइक्रोमैकेनिकल उपकरण में परीक्षण किए गए भू-सामग्री संपर्कों की कतरनी प्रतिक्रिया की सटीकता को उच्च-स्तरीय ट्राइबोमीटर उपकरण से प्राप्त समान संपर्कों के परिणामों की तुलना करके प्रदर्शित किया गया है। परीक्षण निष्कर्ष दिखाते हैं कि कस्टम-निर्मित उपकरण उतना ही सटीक है जितना कि उच्च-स्तरीय ट्राइबोमीटर और भू-सामग्री के माइक्रोमैकेनिकल अंतःक्रिया विश्लेषण के लिए विश्वसनीय है। इसके अतिरिक्त, विभिन्न प्रकार के इंटरफेस संपर्कों और विभिन्न परिस्थितियों के तहत प्रयोग किए गए, ताकि उपकरण की संवेदनशीलता को प्रदर्शित किया जा सके। निष्कर्ष इंगित करते हैं कि उपकरण की कठोरता पर्याप्त है, यह माइक्रोमैकेनिकल व्यवहार को समझने में सहायता करता है और भू-सामग्रियों के जटिल व्यवहार को समझने के लिए आवश्यक प्राथमिक लेकिन महत्वपूर्ण इनपुट्स का आकलन करता है।

माइक्रोमैकेनिकल इंटरफेस कतरनी परीक्षण स्कैन किए गए कणों पर किए गए, जिसमें कणों की औसत सतह खुरदरापन, सामान्य भार, और सतत सामग्री के प्रकार का कण-स्तर पर कतरनी प्रतिक्रिया पर महत्वपूर्ण प्रभाव दिखाया गया। स्पीयरमैन की रैंक सहसंबंध गुणांक विश्लेषण सतत सामग्री की कठोरता और बिना किसी फ़िल्टर के मापे गए कणों की औसत खुरदरापन ($S_{a_particle}$) के बीच एक मजबूत सहसंबंध को प्रदर्शित करता है, जो गैर-दिलेटिव इंटरफेस में कतरनी प्रतिक्रियाओं को प्रभावित करने में उनकी पारस्परिक निर्भरता को उजागर करता है। तीन सतत सामग्रियों में औसत सतह खुरदरापन के प्रति घर्षण गुणांक की प्रतिक्रिया अलग-अलग होती है, जिसमें PVC सबसे उच्च घर्षण गुणांक मान प्रदर्शित करता है, इसके बाद HDPE और ST आते हैं, समान परीक्षण परिस्थितियों के तहत। HDPE का घर्षण गुणांक $S_{a_particle}$ के साथ घातीय वृद्धि दर्शाता है, जो सामान्य भार बढ़ने पर b_p मानों की वृद्धि में परिलक्षित होता है। इसके विपरीत, PVC एक घात संबंध (पावर-लॉ रिलेशनशिप) प्रदर्शित करता है, जहां उच्च $S_{a_particle}$ पर घर्षण गुणांक की वृद्धि दर घट जाती है, जो बढ़ते सामान्य भारों के तहत सतह के न्यूनतम विकृति के कारण होता है। ST में, घर्षण गुणांक $S_{a_particle}$ के साथ लगभग स्थिर वृद्धि दिखाता है, जो डेटा पर रैखिक फिट के लिए स्थिर m मानों द्वारा संकेतित होता है। माइक्रोमैकेनिकल प्रायोगिक डेटा का उपयोग करके विभिन्न मशीन लर्निंग मॉडल लागू किए गए, ताकि इष्टतम प्रिडिक्टिव मॉडल की पहचान की जा सके, जिसमें RF मॉडल ने अन्य मॉडलों को पीछे छोड़ते हुए प्रशिक्षण के लिए $R^2 = 0.94$ और परीक्षण के लिए $R^2 = 0.89$ प्राप्त किया। इसने सभी सत्यापन मानदंडों को पूरा किया और इसे पूरी तरह से स्वीकार्य माना गया।

TABLE OF CONTENTS

CERTIFICATE	i
ACKNOWLEDGEMENT.....	ii
ABSTRACT.....	v
सारांश	ix
TABLE OF CONTENTS.....	xiii
LIST OF FIGURES	xvii
LIST OF TABLES.....	xxiv
LIST OF SYMBOLS AND NOTATIONS.....	xxvi
CHAPTER 1 INTRODUCTION	1
1.1 General.....	1
1.2 Organization of the Thesis	5
CHAPTER 2 LITERATURE REVIEW	6
2.1 Introduction.....	6
2.2 Non-Dilative Interfaces in Geotechnical Engineering.....	7
2.2.1 Load Transfer and Frictional Mechanisms	8
2.2.2 Factors Influencing Shear Response	10
2.2.3 Efforts Made to Comprehend Non-Dilative Interfaces Accurately	15
2.2.4 Importance of Micromechanical Studies	25
2.3 Importance of Data-Driven Insights	27

2.4 Research Gaps and Need for the Study.....	32
2.5 Objectives	33
CHAPTER 3 MATERIALS AND CHARACTERIZATION.....	35
3.1 Introduction.....	35
3.2 Continuum Materials Used	35
3.3 Particulate Materials Used	37
3.3.1 Hardness.....	38
3.3.2 3D Shape Characterization (Macro and Mesoscale features)	39
3.3.3 Roughness Characterization (Microscale features)	61
3.3.4 Geotechnical Properties	62
3.4 Summary	64
CHAPTER 4 INSIGHTS INTO THE GEOTRIBOLOGY OF NON-DILATIVE INTERFACES FROM NOVEL EXPERIMENTAL INVESTIGATIONS	65
4.1 Introduction.....	65
4.2 Testing Program and Materials Used	66
4.3 Interface Direct Shear Tests Enabled with Digital Imaging Technique	68
4.3.1 Testing Methodology	68
4.3.2 Sand-Polymeric Continuum Materials Test Results	74
4.3.3 Sand-Steel Interface Test Results.....	93
4.4 Interface Direct Shear Test with X-ray CT Scanning	95
4.4.1 Testing Methodology	95
4.4.2 Results and Discussion	100

4.5 Summary	110
CHAPTER 5 DEVELOPMENT OF AN APPARATUS FOR DETERMINING MICROMECHANICAL INTERFACE SHEAR PROPERTIES.....	113
5.1 Introduction.....	113
5.2 Custom-built micromechanical interface shear testing apparatus	115
5.2.1 Description of Apparatus	115
5.2.2 Configurations.....	118
5.2.3 Instrumentations and Data Acquisitions	119
5.3 Sample Preparation and Testing Procedure	120
5.3.1 Sample Preparation	122
5.3.2 Testing Procedure.....	124
5.4 Repeatability and Force Correction	125
5.5 Accuracy of Test Results.....	126
5.6 Interface Shear Response of Geomaterial Contacts.....	127
5.6.1 Particle Sliding Condition.....	127
5.6.2 Particle Rolling Condition	133
5.6.3 Imaging Facility	134
5.7 Summary	137
CHAPTER 6 DATA-DRIVEN INSIGHTS INTO THE MICROMECHANICAL SHEAR RESPONSE OF GEOMATERIAL CONTACTS.....	139
6.1 Introduction.....	139
6.2 Materials and Methodology	140

6.2.1 Materials	140
6.2.2 Micromechanical Shear Test Apparatus.....	141
6.2.3 Sample Preparation and Testing Procedure	141
6.2.4 Methodology for Predictive Model Development	142
6.3 Results and Discussion	148
6.3.1 Particle Surface Roughness.....	149
6.3.2 Typical Single Particle-Continuum Materials Interface Test Responses ..	152
6.3.3 Correlation assessment	159
6.3.4 Effect of Particle Contacts on the Interface Friction Coefficient and Shear- Induced Surface Changes.....	161
6.3.5 Performance Evaluation Metrics for Machine Learning Models	171
6.4 Summary	179
CHAPTER 7 CONCLUSIONS.....	181
7.1 Major Findings of the Study	181
7.2 Limitations and Recommendations for Future Work.....	185
References.....	187
LIST OF PUBLICATIONS / PATENT	216
ABOUT THE AUTHOR.....	218

LIST OF FIGURES

Figure 1.1 Schematic illustration of (a) dilative interface system (b) non-dilative interface system (after (Vangla, 2016)).....	2
Figure 2.1. Importance of non-dilative interface system in geotechnical applications (a) landfill liner, (b) friction piles, and (c) cone penetrometer device	8
Figure 2.2. Schematic illustration of (a) adhesion (b) Plowing	10
Figure 2.3. Smooth HDPE Geomembrane—Ottawa Sand Interface Shear Mechanisms (Dove and Frost, 1999)	18
Figure 2.4 Different aspects describing particle shape on the macro, meso and micro levels in (a) 2D and (b) 3D	22
Figure 3.1 Images of continuum materials used (a) HDPE, (b) PVC, (c) AS, (d) ST ..	36
Figure 3.2 Particle size distribution of the sands used in this study	38
Figure 3.3 Images of particulate materials used in this study	38
Figure 3.4 Images of the particulate materials used in the study to assess the proposed algorithm’s effectiveness.....	41
Figure 3.5 Comparison between real particles and 3D meshes obtained by the optical interferometry scanner for (a) crushed aggregates, and (b) pebbles; (c) Illustration of individual Soma sand particles obtained from X-ray CT specimen	41
Figure 3.6 (a) 3D STL file of a crushed aggregate (b) 3D mesh surface of the particle obtained from the STL file without any modifications (c) Region segmentation performed on each point of the unmodified particle mesh	45
Figure 3.7 Flowchart depicting the mesh simplification algorithm used in the study ..	47
Figure 3.8 Sensitivity analysis of volume and roundness of particles with increased mesh simplification.....	49

Figure 3.9 Simplified meshes free from roughness alongside their respective segmentation regions of (a) aggregate, (b) pebble, and (c) Soma sand	50
Figure 3.10 True Sphericity (ψ) vs. Roundness (R) chart plotted for the particles in the study.....	52
Figure 3.11 MII and RDF for aggregates, sand grains, and pebbles used in this study	58
Figure 3.12 Visualizing Particle Shape: MII and RDF space	59
Figure 3.13 Segmented regions of three representative particles of (a) quarry sand, (b) glass beads-1, and (c) glass beads-2	60
Figure 3.14 Microscopic images of (a) quarry sand, (b) glass beads-1, and (c) glass beads-2 with insets at 500x magnification.....	62
Figure 4.1 Advanced interface direct shear apparatus in (a) fixed test setup (b) conventional test setup.....	70
Figure 4.2 Top view of the sliding platform with (a) acrylic sheet and (b) brass plate placed in the slot for experiments with and without image analysis, respectively	71
Figure 4.3 Interface shear response of (a) SA_S and S_GB with HDPE and (b) SA_S and S_GB with AS at 25 kPa and 200 kPa in fixed and conventional test setups; and the failure envelopes of SA_S, R_GB and S_GB with (c) HDPE interfaces (d) AS interfaces	76
Figure 4.4 Displacement field in y-direction at peak at the interface in (a) fixed box and (b) conventional box test setup for SA_S-AS and S_GB-AS interfaces under normal stress of 200 kPa	78
Figure 4.5 Interface shear response of (a) SA_S-HDPE, (b) SA_S-AS, (c) R_GB-HDPE, (d) R_GB-AS, (e) S_GB-HDPE, and (f) S_GB-AS at different normal stresses	79

Figure 4.6 Variation of coefficient of friction with the normal stress for different interfaces of AS and HDPE.....	80
Figure 4.7 Variation of average roughness values with normal stress for different interfaces of AS and HDPE.....	82
Figure 4.8 Post shear images of AS at (a) 25 kPa and (b) 200 kPa and HDPE at (c) 25 kPa and (d) 200 kPa	83
Figure 4.9 Displacement field in y-direction for SA_S-AS under 25 kPa, 100 kPa, and 200 kPa measured at a) half of the peak shear stress, b) peak shear stress, and c) 10 mm	85
Figure 4.10 Displacement field in y-direction for R_GB-AS under 25 kPa, 100 kPa, and 200 kPa measured at a) half of the peak shear stress, b) peak shear stress, and c) 10 mm	86
Figure 4.11 Displacement field in y-direction for S_GB-AS under 25 kPa, 100 kPa, and 200 kPa measured at a) half of the peak shear stress, b) peak shear stress, and c) 10 mm	87
Figure 4.12 Spatial distribution of average roughness in SA_S-AS at (a) 25 kPa (b) 200 kPa.....	88
Figure 4.13 Spatial distribution of average roughness in SA_S-HDPE at (a) 25 kPa (b) 200 kPa.....	88
Figure 4.14 Spatial distribution of average roughness in (a) S_GB-HDPE, (b) R_GB-HDPE, (c) S_GB-AS, (d) R_GB-AS at 200 kPa	90
Figure 4.15 Displacement vectors at peak in (a) S_GB, (b) R_GB, and (c) SA_S at 25 kPa.....	92
Figure 4.16 Interface shear response of (a) SA_S-ST, and (b) S_GB-ST at different normal stresses	94

Figure 4.17 Variation of coefficient of friction with the normal stress for different interfaces of ST	95
Figure 4.18 Experimental setup (a) X-ray CT scanner compartment (b) Modified shear test apparatus	97
Figure 4.19 Schematic diagram of the test setup	98
Figure 4.20 Interface shear response of (a) SA_S-HDPE, (b) SA_S-PVC, (c) S_GB-HDPE, and (d) S_GB-PVC at different normal stresses with and without X-ray CT scanning	102
Figure 4.21 Variation of coefficient of friction with the normal stress for different interfaces of HDPE and PVC.....	103
Figure 4.22 Strain field in shearing direction for SA_S-HDPE under 25 kPa, 100 kPa, and 200 kPa measured at (a) half of the peak shear stress, (b) peak shear stress, and (c) 6 mm	104
Figure 4.23 Strain field in shearing direction for S_GB-HDPE under 25 kPa, 100 kPa, and 200 kPa measured at (a) half of the peak shear stress, (b) peak shear stress, and (c) 6 mm	105
Figure 4.24 Strain field in shearing direction for SA_S-PVC under 25 kPa, 100 kPa, and 200 kPa measured at (a) half of the peak shear stress, (b) peak shear stress, and (c) 6 mm	108
Figure 4.25 Strain field in shearing direction for S_GB-PVC under 25 kPa, 100 kPa, and 200 kPa measured at (a) half of the peak shear stress, (b) peak shear stress, and (c) 6 mm	109
Figure 5.1 Schematic diagram of (a) 2D cross section (at the center of the apparatus along shearing direction), (b) 3D view of the apparatus.....	117

Figure 5.2 Schematic views of (a) sample holder plate for (i) dry condition, (ii) wet condition, and (iii) image capturing (b) particle fixture for (i) sliding, and (ii) rolling condition	119
Figure 5.3 Material samples used in this study (a) particulate materials (b) continuum materials.....	122
Figure 5.4 Final testing configuration of particle-continuum materials for (a) sliding condition, (b) rolling condition, and (c) imaging of geomaterial contact while shearing	124
Figure 5.5 Repeatability of the interface micro shear test results.....	126
Figure 5.6 Correction of the horizontal force during interface shear testing.....	126
Figure 5.7 (a) f_h vs. d_h , and (b) μ_s vs. f_v response for SB-ST interface contacts of tribometer and new apparatus	127
Figure 5.8 Typical f_h vs. d_h response of (A) S_GB-ST, (B) SA_S-ST, (C) S_GB-HDPE, and (D) SA_S-HDPE interface.....	130
Figure 5.9 μ_s vs. f_v for S_GB-ST, SA_S-ST, S_GB-HDPE, and SA_S-HDPE interface contacts	130
Figure 5.10 μ_s vs. f_v response for (A) S_GB-ST, and SA_S-ST, (B) S_GB-HDPE, and SA_S-HDPE interface contacts under dry and wet conditions.....	131
Figure 5.11 Coefficient of sliding friction vs. displacement rate response for S_GB-ST interface at a normal load of 40 N	132
Figure 5.12 Typical responses of S_GB-ST interface contacts (A) f_h vs. d_h , (B) f_v vs. d_h , (C) d_v vs. d_h , and (D) μ_r vs. f_v	134
Figure 5.13 (a) f_h vs. d_h response (b) and (c) Images captured from the bottom of the apparatus while shearing at normal load of 20 N and 80 N, respectively, for SA_S-AS	

interface; (arrow marked in red and blue color on images indicate the location of grooves).....	135
Figure 6.1 Optical images of the typical SA_S particles at the magnification of 50X using a Keyence microscope.....	149
Figure 6.2 Average surface roughness of the sand particles (a) without filter, and with an L-filter of (b) 0.8 mm (c) 0.5 mm (d) 0.25 mm (e) 0.2 mm measured using a Keyence microscope with average (black color line) and standard deviation (red color line)	151
Figure 6.3 Typical (a) shear force / (b) shear stiffness vs. horizontal displacement response plots for interface shear test of single sand particles of varying surface roughness with HDPE.....	154
Figure 6.4 Typical (a) shear force / (b) shear stiffness vs. horizontal displacement response plots for interface shear test of single sand particles of varying surface roughness with PVC	156
Figure 6.5 Typical (a) shear force / (b) shear stiffness vs. horizontal displacement response plots for interface shear test of single sand particles of varying surface roughness with ST.....	158
Figure 6.6 Correlation coefficient matrix heatmap of feature variables and label	160
Figure 6.7 Coefficient of friction vs. particle’s average surface roughness response for HDPE interfaces at different normal loads	163
Figure 6.8 Coefficient of friction vs. particle’s average surface roughness response for PVC interfaces at different normal loads.....	165
Figure 6.9 Coefficient of friction vs. particle’s average surface roughness response for ST under different normal loads	167

Figure 6.10 Shear-induced surface roughness vs. particle's average surface roughness response for HDPE under different normal loads	168
Figure 6.11 Shear-induced surface roughness vs. particle's average surface roughness response for PVC under different normal loads.....	170
Figure 6.12 Shear-induced surface roughness vs. particle's average surface roughness response for ST under different normal loads.....	170
Figure 6.13 Coefficient of friction values box plot for outliers identification.....	172
Figure 6.14 Scatter plots displaying the relationship between observed and predicted values for the test datasets using (a) RF, (b) DTR, (c) MLP, and (d) GAM models..	176

LIST OF TABLES

Table 2.1. Important influencing factors affecting shear behavior of non-dilative interface system	13
Table 2.2 List of published macroscale and mesoscale descriptor formulae	23
Table 2.3 Literature studies reviewed for machine learning models in geotechnical engineering	30
Table 3.1 Properties of geomembranes used in this study	37
Table 3.2 Hardness and roughness values of the continuum materials used in this study	37
Table 3.3 Particles having the same roundness (R) and true sphericity (ψ) yet observed to have a drastic variation in shape	52
Table 3.4 Particles with the same Roundness but significantly different MII	55
Table 3.5 Particles with the same sphericity but significantly different RDF	56
Table 3.6 Morphological characteristics (3D) of particulate materials	61
Table 3.7 Geotechnical properties of the sands used in this study	63
Table 4.1 Test program for advanced interface direct shear test	68
Table 4.2. Scanning condition of the samples in an X-ray CT scanner	99
Table 4.3 Coefficient of friction values for the different interfaces	110
Table 6.1 Performance evaluation indicators	148
Table 6.2 The constants a_e and b_e of the fitted exponential curve on μ vs. $S_{a_particle}$ and R_a vs. $S_{a_particle}$ for HDPE interfaces at different normal loads	164
Table 6.3 The constants a_p and b_p of the fitted power curve on μ vs. $S_{a_particle}$ and R_a vs. $S_{a_particle}$ for PVC interfaces at different normal loads	166
Table 6.4 The constants m and c of the linear fit on μ vs. $S_{a_particle}$ and R_a vs. $S_{a_particle}$ for ST interfaces at different normal loads	168

Table 6.5 Overview of the dataset statistics	171
Table 6.6 Overview of the dataset statistics after excluding the outliers	173
Table 6.7 Statistical metrics for the training dataset	174
Table 6.8 Statistical metrics for the test dataset	175
Table 6.9 Evaluation of machine learning models ranked by their performance on training and testing datasets.	175
Table 6.10 Validation of data-driven models based on the guidelines established by Golbraikh and Tropsha (2002).	178

LIST OF SYMBOLS AND NOTATIONS

F	Total frictional force
$F_{adhesion}$	Adhesion component of frictional force
$F_{plowing}$	Plastic deformation component of frictional force
τ_a	Material shear strength at points of contact
τ_p	Bulk strength of the softer material
A	Real contact area
A_p	Cross-sectional area of the plowed track
W	Applied load
N	Load index
A	Surface area of the particle
A_s	Surface area of the sphere having the same volume as the particle
C	Circumference of the particle
c	Circumference of the circle having the same area as the particle
D_c	Diameter of the smallest circumscribed circle
d	Diameter of the circle has the same area as the particle
D_i	Diameter of the largest inscribed sphere
L	Longest axis dimension of the particle
I	Intermediate axis dimension of the particle
S	Shortest axis dimension of the particle
Z_i	The longest dimension in the i^{th} direction
p_i	$\frac{Z_i}{L + I + S}$
r	Radius of curvature of corner

N	Number of corners
D_k	Diameter of the curvature of the sharpest corner
a	Angle subtended by corner
x	Distance from corner tip to the centre of maximum inscribed circle
D_{s1}, D_{s2}	Diameter of the curvature of the two sharpest corners of particle
$HDPE$	High-density polyethylene
PVC	Polyvinyl chloride
AS	Acrylic sheet
ST	Steel
K_1, k_2	Principal curvatures
k_H	Mean curvature
k_G	Gaussian curvature
SA_S	Sub-angular sand
S_GB	Smooth glass beads
R_GB	Rough glass beads
R_{3D}	3D Wadell roundness
N_i	Initial number of faces
R_i	Initial roundness
V_i	Initial volume
N_{ll}	Lower limit of the number of faces
rf	Reduction factor
MII	Mesoscale interlocking index
RDF	Radial distance factor
R_{corner}	Mean radius of curvature of corner

<i>MIS</i>	Maximum inscribed sphere
<i>R_{MIS}</i>	Radius of curvature of MIS
<i>R</i>	Roundness
ψ	True sphericity
<i>NCAR</i>	Non-corner aspect ratio
<i>CLR</i>	Curvature length ratio
<i>A_x</i>	Voronoi area of vertex x
<i>p</i>	Number of highly concave vertices
<i>q</i>	Number of highly convex vertices
<i>k_x</i>	Curvature of any vertex
<i>k_{MIS}</i>	Curvature of maximum inscribed sphere
<i>x_i</i>	Distance between any vertex (i) and the center of MIS
<i>S_a</i>	Average surface roughness of particles
<i>R_a</i>	Average roughness of continuum material
<i>LVDT</i>	Linear variable differential transformer
<i>DAQ</i>	Data acquisition system
<i>LMS</i>	Linear motion system
<i>DEM</i>	Discrete element method
<i>FEM</i>	Finite element method
<i>f_h</i>	Shear force
<i>d_h</i>	Horizontal displacement
μ_s	Sliding friction coefficient
<i>f_v</i>	Normal load
μ_r	Rolling friction coefficient

<i>RF</i>	Random forest
<i>DTR</i>	Decision tree regressor
<i>MLP</i>	Multilayer perceptron
<i>GAM</i>	Generalized additive models
μ_o	Observed value of interface friction coefficient
μ_p	Predicted value of interface friction coefficient
<i>RMSE</i>	Root mean square error
R^2	Coefficient of correlation
<i>MAPD</i>	Mean absolute percentage deviation
<i>COV</i>	Coefficient of variation
<i>S_{a,particle}</i>	Average surface roughness of particles without filter
<i>a_e, b_e</i>	Exponential curve fit coefficients
<i>a_p, b_p</i>	Power curve fit coefficients
<i>m, c</i>	Linear fit coefficients
<i>Q3</i>	Upper quartile
<i>Q1</i>	Lower quartile
<i>k, k'</i>	Slopes of regression lines for experimental and predicted data
$R_o^2, R_o'^2$	Determination coefficients of the predicted versus observed values and observed versus predicted values
<i>R_s</i>	Stabilization criterion